Update on E12-07-109 to PAC 47:
Large Acceptance Proton Form Factor Ratio Measurements
up to 14.5 GeV^2 Using the Recoil-Polarization Method

E. Cisbani,[1] M. K. Jones,[2] N. Liyanage,[3] L. P. Pentchev,[2] A. J. R. Puckett,[4] and B. Wojtsekhowski[2, *]

(GEp/SBS and Hall A Collaborations)

[1]*INFN, Rome, Italy*
[2]*Jefferson Lab, Newport News, VA, USA*
[3]*University of Virginia, Charlottesville, VA, USA*
[4]*University of Connecticut, Storrs, CT, USA*
(Dated: May 31, 2019)

During the last two decades a number of experiments have made precision measurements of the proton electromagnetic form factor ratio G_{Ep}/G_{Mp} in a wide range of momentum transfer Q^2 using the polarization transfer method. The most important result of these experiments is the dramatic reduction of that ratio with Q^2 between $1 \leq Q^2 \leq 8.5$ GeV^2. As a result, the field of nucleon electromagnetic form factors at large Q^2, connected to the worldwide effort to study Generalized Parton Distributions, has experienced a resurgence in interest and attention. The experiment under discussion, E12-07-109, was approved by PAC32. PAC35 allocated 45 days with a slightly reduced range of momentum transfer (12.5 GeV^2). E12-07-109 received a "High Impact Experiment" designation from PAC41. This document provides an update on the experiment preparation and a brief summary of the progress in the field of nucleon form factors since 2010.

I. INTRODUCTION

The electron-nucleon scattering form factor experiments performed by Hofstadter in the 1950s [1] at low momentum transfer were successfully analyzed in the framework of Rosenbluth theory [2], which uses the one-photon-exchange approximation. In 1957 Akhiezer [3] and collaborators suggested that at Q^2 higher than a few GeV^2, a polarized electron beam experiment would provide much better accuracy than the Rosenbluth method for determination of the Dirac (F_1) and Pauli (F_2) form factors. Similar ideas were also proposed later by other authors [4, 5]. Experimental realization of double polarization measurements at momentum transfers of several GeV^2 became possible in the 1990s with the advent of 100% duty factor electron accelerators. In addition to the beam-target double polarization observable, the spin transfer reaction could be used as suggested in Refs. [6, 7]. The experimental technique for such a measurement (recoil proton polarimetry) was developed in much detail in nucleon-nucleon scattering experiments, see e.g. Ref. [9, 10]. High accuracy of the G_E^p/G_M^p measurement became possible after the ratio P_t/P_l method was introduced in several electron-nucleon scattering experiments, see [11–14]. The ratio is not sensitive to the polarization of the electron beam or the analyzing power of the polarimeter, which would otherwise be a dominant source of systematic uncertainty in the experimental result. The ratio method for the G_E^p measurement in the spectrometer focal plane has been developed in many aspects in Ref. [12]. The surprising results of the GEp-I [15, 16] and GEp-II/III [17, 18] experiments in Hall A/C are among the most widely cited results from the 6 GeV era of CEBAF operations and launched major worldwide efforts to both extend the proton and neutron electric form factor measurements to the highest practically achievable Q^2, and to understand the implications of the high-Q^2 form factor data for nucleon structure and dynamics in QCD. These results also spawned parallel efforts to measure and predict ep scattering observables directly sensitive to the two-photon-exchange effects thought to be responsible for the disagreement between extractions of G_E^p from absolute cross section data and polarization measurements [19].

II. THE STATUS AND ISSUES OF THE ELASTIC ELECTRON-NUCLEON FORM FACTORS

Since this experiment was proposed in 2007, JLab Hall C experiments E04-108 [20, 21], and E04-019 [21, 23] have made the next major advance with the measurement of the G_E^p/G_M^p ratio up to 8.5 GeV^2 and the precise measurement of the ϵ dependence of the ratio to constrain the two-photon contribution at the moderately large Q^2 of 2.5 GeV^2. In the proposal update to PAC35 we wrote "A common thread in virtually all of the theoretical explanations of the Q^2-dependence of GEp/GMp is an important role for quark orbital angular momentum (quark OAM) in the nucleon's dynamics. What is remarkable is that evidence for quark OAM has begun showing up in other processes as well." Soon after that, new experimental data from the Hall A G_E^n/G_M^n measurement [24] led to the observation [25] that so-called logarithmic scaling [26] of the F_2^p/F_1^p ratio is not due to the quark OAM but likely due to a very large change in the ratio of the d-quark to u-quark contributions to the form factors when the momentum transfer varies from 1 GeV^2 to 3.4 GeV^2. Indeed, the $F_{1,d}^p/F_{1,u}^p$ ratio drops in that range of Q^2 by a factor of 3! This unexpected feature is consistent with calculations based on the Dyson-Schwinger Equation method [27]. The pQCD-based phenomenological models are not applicable to exclusive processes such as elastic ep scattering in the range of momentum transfer currently accessible to experiment. The phenomenological models of Generalized Parton Distributions (GPDs) [28] are very useful for connecting different reactions and even "predicted" (using one of several proposed Ansätze) the observed drop of $F_{1,d}^p/F_{1,u}^p$ [29]. We note that the GPDs provide a powerful opportunity to determine quark angular momentum in a model-independent fashion. Also, the elastic form factors provide a powerful check of lattice QCD. *Ab initio* lattice calculations of ground-state form factors are making impressive progress (see, e.g., Ref. [30]), and the comparison of these results with experimental measurements is extremely important.

In the years following the discovery by Jones *et al.* [15], it is not surprising that models evolved that explained well the existing proton data. It is also not surprising that these models diverge strongly at high-Q^2, where there is no data to constrain the calculations. Higher values of Q^2 also offer the advantage of certain theoretical simplifications. For example, the role of vector mesons is suppressed at higher Q^2, as are higher Fock states in the phenomenological models of GPDs. At high Q^2 there is increased clarity and increased discovery potential, and GEp/SBS provides an excellent opportunity to explore this region, see Fig. 1. By going to Q^2=12.5 (GeV/c)^2, the trend of G_E^p/G_M^p should become clear, *but only if the data have sufficient precision.* Such precision is offered by the present experiment, which has a figure-of-merit 10 times higher than any other proposed or possible experiment using existing or planned equipment other than the SBS spectrometer.
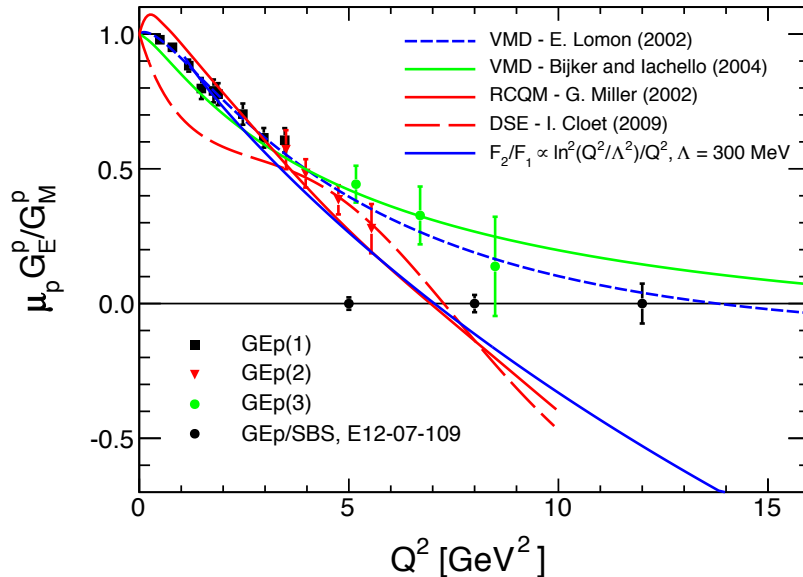
FIG. 1. Published G_{Ep}/G_{Mp} data (recoil polarimetry only) and projected accuracy of this experiment.

III. THE CONCEPT OF THIS EXPERIMENT

We will measure the polarization transfer to the recoiling proton in the elastic scattering of longitudinally polarized electrons with energies up to 11 GeV from a liquid hydrogen target, $H(\vec{e},e'\vec{p})$. Polarization transfer observables provide direct access to the G_E^p/G_M^p ratio as proposed in Ref. [3] and described below. In the one-photon exchange approximation, the scattering of longitudinally polarized electrons from unpolarized protons results in a transfer of polarization to the recoiling protons with two components, P_t perpendicular to, and P_ℓ parallel to the proton momentum in the scattering plane [7, 8]:

$$P_t = -\sqrt{\frac{2\epsilon(1-\epsilon)}{\tau}}\frac{G_E G_M}{\sigma_{red}},$$
$$P_\ell = \sqrt{(1-\epsilon^2)}\frac{G_M^2}{\sigma_{red}} \tag{1}$$

where the reduced cross section $\sigma_{red} \equiv G_M^2 + \frac{\epsilon}{\tau}G_E^2$, $\epsilon \equiv [1+2(1+\tau)\tan^2\frac{\theta_e}{2}]^{-1}$, θ_e is the lab electron scattering angle, and $\tau \equiv Q^2/4M_p^2$.

Measuring these two components simultaneously and taking their ratio gives the ratio of the form factors

$$\frac{G_E}{G_M} = -\frac{P_t}{P_\ell}\sqrt{\frac{\tau(1+\epsilon)}{2\epsilon}} \tag{2}$$

Using the double-polarization technique, the form factor ratio G_E/G_M at a given Q^2 can be obtained without measuring the absolute cross sections and without a change of beam energy or detector angle, thus eliminating important sources of systematic uncertainties. Note that the analyzing power of the polarimeter and the electron beam polarization that affect an independent absolute determination of P_t and P_ℓ cancel exactly in Eq. 2, and thus do not need to be known particularly well. They do affect the size of the measured asymmetries, however, so they still need to be maximized to increase the experimental figure-of-merit.

In measuring the nucleon G_E/G_M ratio, this method avoid difficulties of the Rosenbluth separation method at high momentum transfer, which is based on ϵ dependence of the cross section $\propto (G_M^2 + \frac{\epsilon}{\tau}G_E^2)$ dominated at high Q^2 by G_M^2 and has also relatively large part originated from the two-photon effects.

The most effective realization of the double-polarization approach for large momentum transfer G_{Ep}/G_{Mp}-ratio experiments was proposed in Ref. [12]. That realization is based on the measurement of the proton polarization following the precession of the proton spin in a magnetic spectrometer, which rotates the longitudinal component P_ℓ

into a normal component P'_n which can be measured using a secondary analyzing reaction. This provides directly the ratio of the polarization components of the proton and has a high figure-of-merit as well as a cancellation of most systematic uncertainties related to the polarimeter analyzing power and efficiency.

There are two major challenges facing an experiment at high momentum transfer: the small elastic scattering cross section and the low analyzing power of the polarimeter. These lead to a very long data taking time required for a precision experiment due to an experimental figure-of-merit that scales approximately as Q^{-16}. To overcome the rapidly decreasing figure-of-merit, the luminosity and the solid angle for detection of the scattered proton need to be as large as practically possible. At large Q^2, the selection of the elastic ep channel in the presence of dominant inelastic backgrounds requires coincident detection of both electron and proton. The kinematics of high-Q^2 elastic ep scattering are such that the proton recoils at rather forward scattering angles, where it is non-trivial to locate a large solid-angle proton arm, and detection of the scattered electrons in an even larger solid angle is needed to match the acceptance of the proton arm. To achieve this cost-effectively necessitates the use of an electromagnetic calorimeter for electron detection. Lead-glass has been the detection medium of choice for electron calorimetry in previous experiments of this type, as it provides the needed energy, spatial, and timing resolution at moderate cost. However, the background radiation level in the calorimeter at the required luminosity leads to a fast degradation of the transparency of lead glass and, therefore, the energy resolution of the calorimeter.

The solution to these challenges, which we put forward in 2007, took advantage of the high rate capability of a tracking device (GEM) invented by F. Sauli in 1997 [22], which allowed us to develop an open magnetic spectrometer with a tracker in direct view of the target. The GEM-based tracker of the polarimeter was complemented by a well segmented hadron calorimeter for a high threshold trigger. The unusual concept of a spectrometer magnetic system in which the beam line goes partly through the yoke of the analyzing magnet, and the use of a large dipole, allowed us to create an apparatus with ten times larger solid angle at large Q^2 than what could be achieved using conventional magnetic spectrometers. The solution to calorimeter radiation damage was found by means of continuous annealing using moderately elevated temperature of the crystals.

IV. PROGRESS WITH THE EXPERIMENT PREPARATION

JLab management organized two reviews of the SBS concepts in 2008 and 2010 and formulated an approach to a funding profile as SBS projects needed. Funded by DOE, the SBS projects include construction of the equipment needed for all three form factor experiments: GEp, GEn, and GMn. These funded projects were fully and successfully completed in 2016. The commissioning and preparation of the experiment is proceeding. Some dependencies are still in the construction/preparation stage. Here we present briefly the full scope and status of the GEp experiment related items.

A. SBS magnet:

All elements of the magnet and beam line have been constructed. Test assembly of the magnet yoke and the platform have been done in Test Lab. The 2 kA power supply unit has been tested in Hall A. The plan is to install the magnet on the right side of Hall A (looking from the target to the beam dump) as shown in Fig. 2.

B. LH2 cryotarget:

The original proposal asked for a 40-cm long liquid hydrogen target. Updated GEANT4-based simulations of the counting rates have shown that a slightly shorter target of 30 cm length will be adequate for the GEp experiment, while advantageously reducing the background rate in the GEM detectors by 35%[1].

C. SBS GEM chambers:

All modules of the GEM chambers and associated electronics have been constructed. The GEM chambers of the polarimeters (10 planes each of 200 cm x 60 cm from the UVa group) are under assembly in the JLab clean room

---

[1] Detailed GEANT4 simulations have shown that the background rate in the front tracker GEMs increases non-linearly with target length, scaling approximately as $L_{tgt}^{3/2}$.
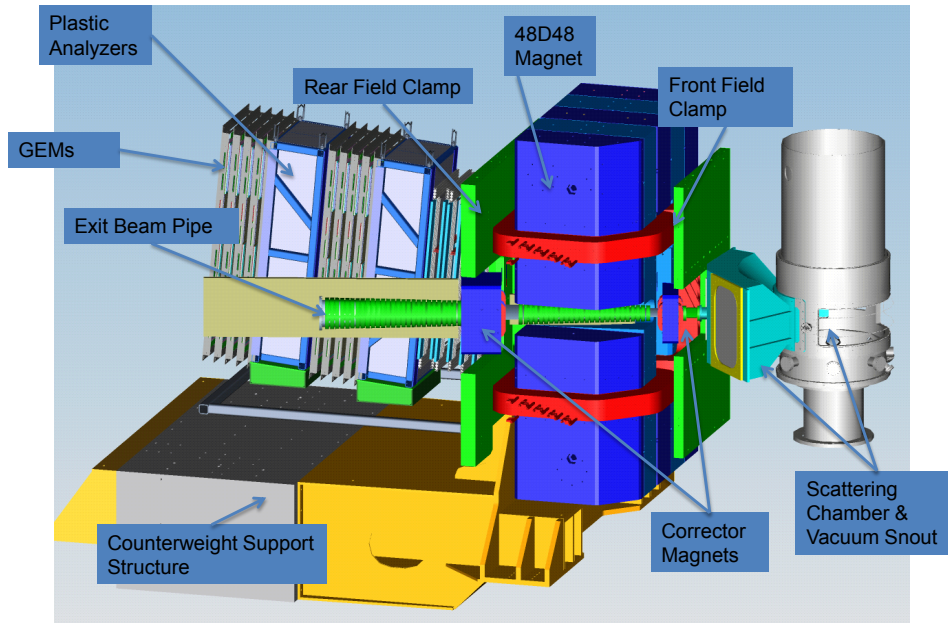
FIG. 2. The layout of the SBS proton arm for the GEp experiment in Hall A, not including the hadron calorimeter HCAL.

for final commissioning. The GEM chambers of the front tracker (six planes each of 150 cm x 40 cm from the INFN group) are under preparation in Test Lab. A high rate test of the UVa GEM modules will be performed in summer 2019 in the HRS focal plane during the PREX experiment.

D. ECAL for the electron arm:

This detector consists of 1737 lead-glass blocks (42.5 x 42.5 x 340 mm^3) viewed via 150-mm long light guides by FEU-84 PMTs (reused from previous experiments). The detector will be located inside a custom oven ($T = 225°$C) to allow constant annealing of the radiation damage during data taking. A complete test of such a method was successfully performed using tagged electrons in Hall A. The high temperature frame and all hardware for the 9-block "supermodules" have been constructed by the NCCU/Yerevan/JLab team. By mid May of 2019 more than 60 out of 193 "supermodules" had been assembled (see an example in Fig. 3). Several thousand FEU-84 PMTs were tested and 2000+ PMTs passed the requirement (JMU team). The PMT HV bases are under modification which is needed due to the ECAL geometry.

E. HCAL for the proton arm:

The hadron calorimeter modules (total of 288) have been designed and constructed by the CMU/Catania team. All four quadrants of the detector were assembled in the Test Lab. Figure 4 shows a view of the detector. Cabling of the electronics is about 66% completed. Results from the cosmic tests performed in summer-fall 2018 are in good agreement with expectations.

F. CDET for the electron arm:

The CDET (Coordinate Detector) consists of 2,400 narrow scintillator counters. CDET allows us to measure the vertical coordinate of the scattered electron several times more precisely than using ECAL alone, which is critical to the exploitation of the two-body exclusive kinematics to aid the track reconstruction in the proton arm in the expected high-rate environment. The detector has two layers with three "modules", consisting of 400 counters each, per layer. All components have been produced by the ISU team. Cosmic ray commissioning of two of the six modules has been completed by the CNU team. Front-end discriminators were made by Glasgow University collaborators.
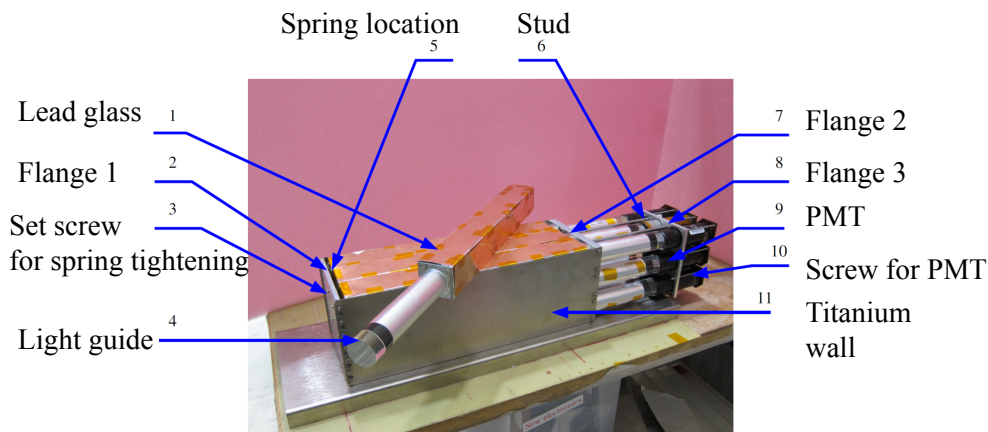
FIG. 3. The ECAL supermodule which includes 9 lead-glass blocks coupled to PMTs by extended cylindrical light-guides.
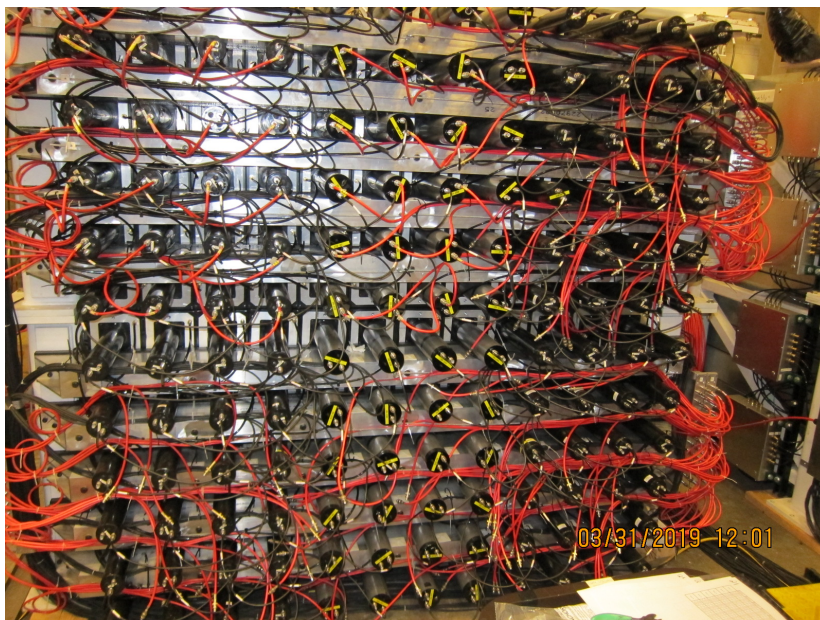

FIG. 4. Two HCAL quadrants in the Test Lab area.

The readout electronics for CDET is based on available FASTBUS 1877s TDCs. Also, some 1881m ADCs are used on the commissioning stage.

G.   GEp trigger/DAQ:

The trigger for the GEp experiment will rely on a coincidence between the single-arm triggers of the electron and proton arms, with loose two-body kinematic correlations implemented at the trigger level to reduce the accidental coincidence rate and manage the high data rate from the GEMs. The single-arm trigger for ECAL will re-use most of the eight-channel analog summing units from GEp-III, allowing us to form an efficient trigger based on summing four groups of eight blocks each, with each 8-block sum combining the signals from 4 (vertical) × 2 (horizontal) lead-glass

blocks. The 32-block sums will be formed from 2×2 groupings of eight-block sums, such that each 32-block sum will combine the signals from a grouping of 8 (vertical) $\times$ 4 (horizontal) lead-glass blocks. The trigger logic groupings are larger in the vertical direction since the elastic event rate and the scattered electron energy are approximately independent of the vertical position in the electron calorimeter. Adjacent 32-block sums will overlap by one eight-block sum in both the vertical and horizontal directions, allowing for a highly-efficient single-arm trigger at high thresholds of up to 80-90% of the elastically scattered electron energy. Most of the ECAL electronics, including FASTBUS 1881m ADCs and LeCroy 1468 high voltage units are prepared for commissioning. The front-end electronics for ECAL (analog summers and discriminators) are in preparation.

The HCAL signals will be read out using Flash ADCs, and the single arm trigger for HCAL will be formed digitally in an FPGA based logic unit from all possible overlapping sums of 4×4 modules, of which there are 189 in total given the 12×24 rectangular layout of the HCAL detector. Two-body kinematic correlations will be implemented in a "level 2" coincidence trigger between the $\approx$220 32-block sums from ECAL and the 189 16-module sums from HCAL, by accepting only events with at least one ECAL trigger sum above threshold in coincidence with an HCAL trigger sum above threshold within a restricted range consistent with two-body ep elastic kinematics.

H.   GEp simulation/analysis software:

The Software/Simulation group (UConn/ANL team) within the SBS collaboration developed a fully detailed and realistic MC model (see Fig. 5) in the framework of Geant4 and is continuing development of the analysis software. This GEANT4 model has been used to evaluate event rates, polarimetry performance, and projected uncertainties in the final proton G_E/G_M ratio. It has also been used to evaluate the performance of the coincidence trigger logic described above in terms of both efficiency and counting rate, and to estimate the background rates and occupancies of the individual detectors. This updated Monte Carlo with full description of the geometry, detector performance, and
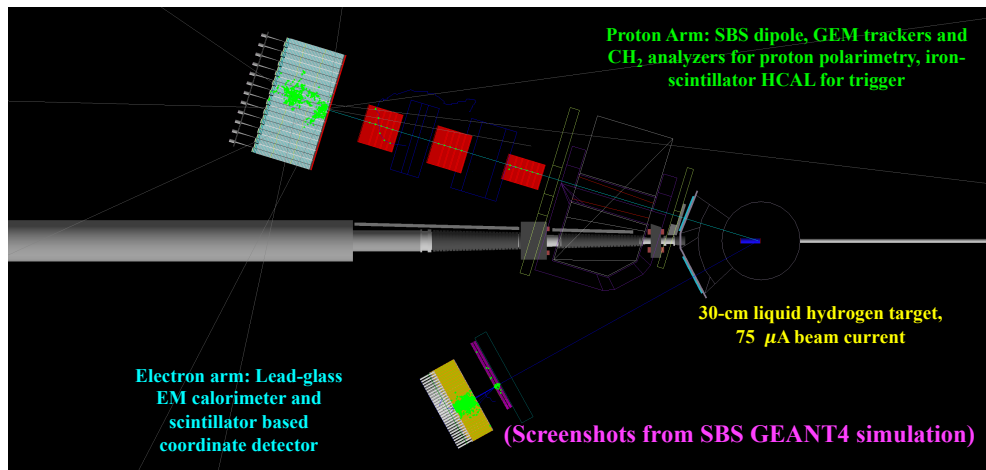

FIG. 5. The top view of the e-p scattering event and the GEp/SBS Geant4 model.

magnetic field was used to update the projected statistical uncertainties in the proton FF ratio under the following assumptions:

- 75 μA beam

- 30-cm liquid hydrogen target

- $\vec{p}$ + CH$_2$ analyzing power angular and momentum dependence parametrized from the fits to GEp-III data published in Ref. [21]. Note that this involves an extrapolation to higher proton momenta.

- 85% electron beam polarization

- SBS dipole field strength scaled with proton momentum, for a constant central bend angle of approximately $5°$, which leads to optimal acceptance, but different precession angles for each Q^2.

- *ep* Born cross sections and polarization transfer components calculated using the "Global Fit II" proton form factor parametrization from the appendix of Ref [21].

The final-state particles in elastic *ep* scattering events were generated in a range of angles sufficient to populate the full SBS acceptance, and tracked through the entire GEANT4 setup. Event rates were then computed according to the acceptance-convoluted scattering cross sections. A simplified approximation of the coincidence trigger was implemented by requiring the total energy deposition in the electron (hadron) calorimeter to be above $\sim 80\%$ (50%) of the mean energy deposited by an elastically scattered electron (proton). Note that because the hadron calorimeter is located behind the polarimeter, some elastically scattered proton events fall below the trigger threshold due to large energy losses and/or large-angle scatterings in the CH_2 analyzers. However, these events have low analyzing power and the HCAL trigger has high efficiency for the events of interest. Events with a single charged track in either set of rear GEMs with "transverse momentum" $p_T \equiv p_p \sin \vartheta_{FPP}$ in the range $0.06 \leq p_T \leq 1.2$ GeV were selected as "good" events for polarimetry, and the analyzing power was evaluated according to a parametrization of the GEp-III data. The statistical figure of merit defined as

$$\mathcal{F} \equiv \sum_{i=1}^{N_{event}} \left(P_e A_y(p_p, p_T) \right)^2 , \tag{3}$$

with P_e the beam polarization and A_y the analyzing power, was evaluated for each of the three proposed kinematics, scaling the number of simulated events to the full beam time request. The statistical uncertainty in each of the two measured proton polarization components at the focal plane of SBS is approximately given by:

$$\Delta P_{x,y}^{FPP} = \sqrt{\frac{2}{\mathcal{F}}} \tag{4}$$

The uncertainties of the polarization components at the target were evaluated by means of the ideal dipole approximation to the spin precession, in which $P_x^{FPP} \approx -P_\ell \sin \chi$, with $\chi = \gamma \, \kappa_p \, \theta_{bend}$ the precession angle relative to the proton trajectory, and $P_y^{FPP} \approx P_t$. The A_y^2-weighted, acceptance-averaged values of P_t, P_ℓ, G_E/G_M, $\sin \chi$, and the kinematic factor $\sqrt{\tau(1+\epsilon)/2\epsilon}$ were evaluated using the chosen form factor parametrization, and finally the statistical uncertainty in the ratio $R \equiv \mu G_E/G_M$ was computed from the standard error propagation formula for a ratio:

$$\left(\frac{\Delta R}{R} \right)^2 = \left(\frac{\Delta P_t}{P_t} \right)^2 + \left(\frac{\Delta P_\ell}{P_\ell} \right)^2 \tag{5}$$

The uncertainties shown in Table I reflect all the aforementioned assumptions, plus the additional assumption that the combined reconstruction efficiencies of all the individual detectors will lead to a global event reconstruction efficiency of 70%, including DAQ dead-time. This is a conservative estimate based on prior experience with the operation of open-geometry detectors at high luminosity in Halls A and C. Note that scaling the SBS dipole field strength with proton momentum leads to smaller precession angles at lower Q^2, reducing somewhat the magnitude of the asymmetry. However, because P_ℓ is approximately ten times as large as P_t or more for all the kinematic settings of E12-07-109, the uncertainty in the ratio G_E/G_M is nevertheless dominated by the uncertainty in P_t, meaning the less-than-optimal precession angle for the two lower-Q^2 settings does not meaningfully increase the uncertainty in the G_E/G_M ratio.

As an aside, it is worth noting that by preferentially selecting high-energy, forward-angle secondary scattering events in the CH_2 analyzers, the HCAL-based trigger may actually *increase* the effective analyzing power of the event sample used for polarimetry relative to GEp-I/II/III, for which the trigger was totally unbiased with respect to interactions in the analyzer and the angular distribution of the totally inclusive event sample in the polarimeter was analyzed based on the measured scattering angles of charged-particle tracks, regardless of the energy of those tracks. However, this increase is speculative and unproven, and the projections presented in this proposal update document assume that the analyzing power of single-track events will be the same as that of the single-track events reconstructed in GEp-III [21], assuming that the linear dependence of the maximum analyzing power can be extrapolated to the higher proton momentum of GEP-SBS.

V. TIME LINE OF THE EXPERIMENT PREPARATION

The internal Hall A projected schedule currently places the production run for this experiment in 2022. Most of the equipment items of the GEp experiment will be used during the GMn formally scheduled to be installed in 2020.
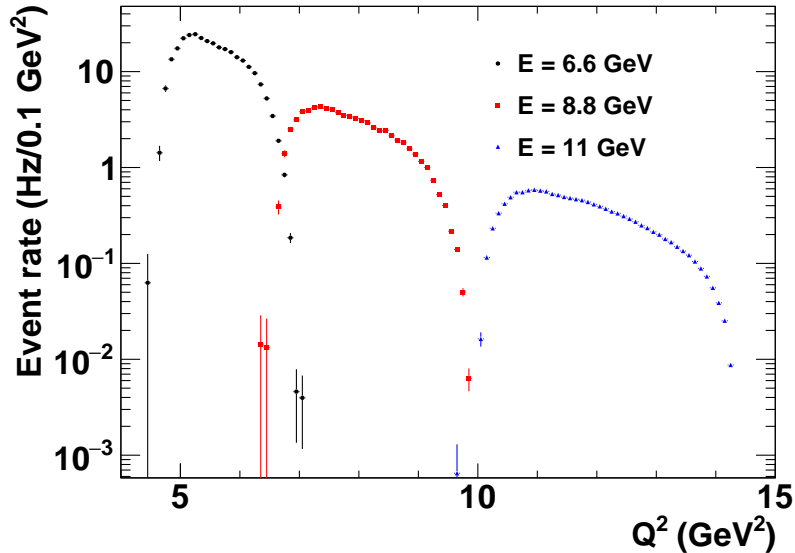
FIG. 6. Acceptance-convoluted elastic ep coincidence event rate as a function of Q^2 for all three kinematic settings of E12-07-109, based on approximate ECAL and HCAL trigger thresholds. Settings are $E = 6.6$ GeV (black circles), $E = 8.8$ GeV (red squares), and $E = 11$ GeV (blue triangles). See Table I for details.

Preparations of the ECAL detector are on track to be ready for a move into Hall A after completion of the GEn experiment in late 2021 or early 2022, as the experimental schedule defines.

VI. SUMMARY AND BEAM TIME REQUEST

The updated kinematical settings and projected accuracies are shown in Table I. Figure 6 shows the event rate as a function of Q^2 within the combined two-arm coincidence acceptance of each kinematic setting. This experiment

TABLE I. Kinematics, projected accuracy and beam time allocations. The projected statistical uncertainties in the form factor ratio include the assumption of 70% overall event reconstruction efficiency due to the combined efficiencies of the individual detectors, including DAQ dead-time.

E_{beam}, GeV	Q^2 range, GeV^2	$\langle Q^2 \rangle$ GeV^2	θ_{ECAL} degrees	$\langle E'_e \rangle$, GeV	θ_{SBS} degrees	$\langle P_p \rangle$ GeV	$\langle \sin \chi \rangle$ degrees	Event rate Hz	Days	$\Delta (\mu G_E/G_M)$
6.6	4.5-7.0	5.5	29.0	3.66	25.7	3.77	0.72	291	2	0.029
8.8	6.5-10.0	7.8	26.7	4.64	22.1	5.01	0.84	72	11	0.038
11.0	10.0-14.5	11.7	29.0	4.79	16.9	7.08	0.99	13	32	0.081

has projected precision which is sufficient for discrimination between existing form factor models on the level of 4 to 5 sigma (see Fig. 1) and helps very significantly to develop understanding of nucleon structure and modeling of the GPDs in the large momentum transfer sector. We request the PAC to re-approve the current beam time allocation of 45 days of beam on target.

[1] R. Hofstadter, Rev. Mod. Phys. **28**, 214 (1956).
[2] M. N. Rosenbluth, Phys. Rev. **79**, 615 (1950).
[3] A. I. Akhiezer, L. N. Rozentsveig, and I. M. Shumushkevich, Zh. Eksperim. i Teor. Fiz **33**, 76 (1957); Sov. Phys. JETP **6**, 588 (1958).
[4] J. H. Scofield, Phys. Rev. **113**, 1599 (1959).
[5] N. Dombey, Rev. Mod. Phys. **41**, 236 (1969).

[6] A. I. Akhiezer and M. P. Rekalo, Dokl. Akad. Nauk Ser. Fiz. **180**, 1081 (1968); Sov. Phys. Dokl. **13**, 572 (1968).

[7] A. I. Akhiezer and M. P. Rekalo, Fiz. Elem. Chast. At. Yad. **4**, 662 (1973); Sov. J. Part. Nucl. **3**, 277 (1974).

[8] R. G. Arnold, C. E. Carlson, and F. Gross, Phys. Rev. **C23**, 363 (1981).

[9] R. Diebold, D. S. Ayres, S. L. Kramer, A. J. Pawlicki, and A. B. Wicklund, Phys. Rev. Lett. **35**, 632 (1975).

[10] H. Spinka *et al.*, Nucl. Instrum. Meth. **211**, 239 (1983).

[11] C. F. Perdrisat, V. Punjabi, *et al.*, "Cebaf proposal 89-014 update," (1992).

[12] C. F. Perdrisat, V. Punjabi, *et al.*, "Cebaf proposal 93-027," (1993), `https://www.jlab.org/exp_prog/proposals/93/PR93-027.pdf`.

[13] R. Madey *et al.*, "Bates proposal e89-04 update," (1994).

[14] M. Ostrick *et al.*, Phys. Rev. Lett. **83**, 276 (1999).

[15] M. K. Jones *et al.* (Jefferson Lab Hall A), Phys. Rev. Lett. **84**, 1398 (2000), arXiv:nucl-ex/9910005 [nucl-ex].

[16] V. Punjabi *et al.*, Phys. Rev. **C71**, 055202 (2005), [Erratum: Phys. Rev.C71,069902(2005)], arXiv:nucl-ex/0501018 [nucl-ex].

[17] O. Gayou *et al.* (Jefferson Lab Hall A), Phys. Rev. Lett. **88**, 092301 (2002), arXiv:nucl-ex/0111010 [nucl-ex].

[18] A. J. R. Puckett *et al.*, Phys. Rev. **C85**, 045203 (2012), arXiv:1102.5737 [nucl-ex].

[19] S. K. Blau, Physics Today **70**, 14 (2017).

[20] A. J. R. Puckett *et al.*, Phys. Rev. Lett. **104**, 242301 (2010), arXiv:1005.3419 [nucl-ex].

[21] A. J. R. Puckett *et al.*, Phys. Rev. **C96**, 055203 (2017), arXiv:1707.08587 [nucl-ex].

[22] F. Sauli, Nucl. Instrum. Meth. A **386**, 531 (1997). doi:10.1016/S0168-9002(96)01172-2

[23] M. Meziane *et al.* (GEp2gamma), Phys. Rev. Lett. **106**, 132501 (2011), arXiv:1012.0339 [nucl-ex].

[24] S. Riordan *et al.*, Phys. Rev. Lett. **105**, 262302 (2010), arXiv:1008.1738 [nucl-ex].

[25] G. D. Cates, C. W. de Jager, S. Riordan, and B. Wojtsekhowski, Phys. Rev. Lett. **106**, 252003 (2011), arXiv:1103.1808 [nucl-ex].

[26] A. V. Belitsky, X.-d. Ji, and F. Yuan, Phys. Rev. Lett. **91**, 092003 (2003), arXiv:hep-ph/0212351 [hep-ph].

[27] C. D. Roberts, M. S. Bhagwat, A. Holl, and S. V. Wright, *Hadron Structure and Nonperturbative QCD. Proceedings, 44. Internationale Universitätswochen für theoretische Physik: Schladming, Austria, February, 2006*, Eur. Phys. J. ST **140**, 53 (2007), arXiv:0802.0217 [nucl-th].

[28] M. Diehl and P. Kroll, Eur. Phys. J. C **73**, 2397 (2013).

[29] M. Diehl, T. Feldmann, R. Jakob, and P. Kroll, Eur. Phys. J. **C39**, 1 (2005), arXiv:hep-ph/0408173 [hep-ph].

[30] A. J. Chambers *et al.* (UKQCD, QCDSF, CSSM), (2017), arXiv:1702.01513 [hep-lat].

[31] A. J. R. Puckett *et al.* (GEp-III, GEp-2Gamma), Nucl. Instrum. Meth. **A910**, 54 (2018), arXiv:1707.07750 [nucl-ex].